Fire Safety Journal 133 (2022) 103645

Contents lists available at ScienceDirect

Fire Safety Journal

journal homepage: www.elsevier.com/locate/firesaf

Fast moving smoldering fronts in thin liquid fuel films dispersed on inert porous media

Sveinung Erland *, Runald Meyer, Bjarne C. Hagen

Western Norway University of Applied Sciences, Bjørnsonsgate 45, Haugesund 5528, Norway

ARTICLE INFO

Keywords:
Smoldering propagation velocity
Liquid fuel films
Inert porous media
Pyrolysis oil
Cotton
Double fronts

ABSTRACT

An experimental study of smoldering in thin layers of pyrolysis oil on an inert substrate of calcium silicate boards has been conducted. The smoldering fronts propagated with velocities up to 0.4 mm/s, which is significantly faster than other types of smoldering without forced air flow. The smoldering propagation velocity increased both with thinner layer of pyrolysis oil and higher initial fuel temperature. Our experimental observations are in close correspondence with a theoretical model based on energy balance, where the availability of oxygen at the substrate surface is the main limiting mechanism. Both the front peak temperature and the front width are correlated to the initial fuel temperature. We also report observations of instability phenomena, including double fronts propagating in close succession. The temperature dynamics were observed by high resolution infrared thermography. The findings contribute to the understanding of the governing mechanisms of smoldering combustion of liquids on inert media, and in particular the fast smoldering fronts that have been observed along the surface of porous insulating materials in experiments with smoldering cotton.

1. Introduction

Smoldering is a slow form of combustion that often occurs in biomass such as wood pellets or peat, or in other materials forming char as it burns [1,2]. Smoldering has also been observed to occur in textiles impregnated with low volatile liquids such as linseed oil [3], and in oil soaked lagging [4,5]. This type of smoldering of liquid fuels represents a risk in, e.g., the petroleum industry when flammable liquids that have leaked into pipeline insulation are ignited. Interestingly, smoldering of liquid fuels has also found some industrial applications, such as soil remediation and enhanced oil recovery [6–8].

The combustion process is flameless, and permeable mediums like fibers, grains and porous matrices often provide the combination of oxygen supply and thermal insulation necessary for a self-sustaining process to occur. While the main smoldering reaction usually occurs at a certain depth within the condensed fuel, self-sustaining smoldering in solid fuels can under certain conditions also occur in very thin layers that are exposed to air [9–11]. Liquid fuels of low volatility are also prone to smoldering when the fuel is dispersed in a rigid, porous substrate [3]. This could potentially include thermally insulating materials like mineral wool used for pipeline lagging and calcium silicate boards that are commonly used as building materials.

The experimental conditions that are the basis for this article are presented in Table 1. The literature on smoldering of liquid fuel in inert mediums is relatively scarce, but in most cases the smoldering fuel has been deposited deep into a thick substrate, as for oil-soaked lagging [4,5,12], various fuels in soil [7,13–17] and oil in sedimentary rocks [6,8,18–20]. Except from in the oil-soaked lagging, forced air flow through the substrate is in most cases required to sustain the smoldering process. We demonstrate that the smoldering also can occur at the surface of inert materials — without forced air flow, but with air supplied to the surface by natural convection. Experiments with solid fuels with somewhat similar conditions have been performed, e.g., with thin layers of horizontally aligned paper both without [10,21] and with [22,23] forced air flow. For thicker samples of solid fuels, smoldering experiments have been conducted both with horizontal and vertical alignment of the fuel (see overview in Ref. [1]). We have chosen horizontal alignment, which we consider to be less complex than the vertically aligned case.

Finally, while temperature measurements in the literature are most often performed by thermocouples (a notable exception is found in, e.g., Ref. [24]), we exploit the quasi-2D conditions of surface combustion and use thermography, which enables far more detailed capturing of the temperature variations, both in time and space, including the detection of fluctuating double fronts with millimeter-scale precision. Notice that our experimental conditions are quite different from the situation arising in smoldering of oil-soaked lagging, but the conditions

* Corresponding author.
E-mail address: sver@hvl.no (S. Erland).

https://doi.org/10.1016/j.firesaf.2022.103645
Received 21 March 2022; Received in revised form 30 June 2022; Accepted 26 July 2022
Available online 1 August 2022

Table 1
The experimental conditions of the current study are to the author's knowledge quite different from those found elsewhere in the literature (see comparisons in the main text).

Experimental set-up	Condition
Fuel	Liquid (pyrolysis oil)
Substrate	Inert porous material (calcium silicate)
Location of smoldering	At substrate surface
Air supply	By natural convection (no forced flow)
Smoldering direction	Horizontal alignment
Measurements	Thermography

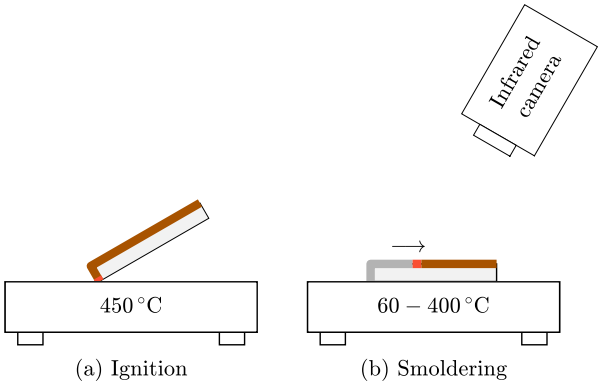

Fig. 1. Schematics of the experimental setup (not to scale). (a) Ignition: Pyrolysis oil has been applied to two faces of the calcium silicate block ($90 \times 50 \times 3$ mm^3). The fuel (fuse) at the bottom edge of the narrow face is ignited at the hot plate (left, 450 °C). Then the smoldering front creeps around the edge to the main face. (b) The sample is transferred to a second hot plate (right), where the sample stabilizes to temperatures governed by the set temperature of the hot plate. The front propagation is observed by infrared camera.

could be similar to other situations that can occur during actual fire scenarios, as outlined in Section 5.

Smoldering is known to propagate as a front where most of the oxidation takes place in a limited zone with increased temperature. Heat is conducted to a pyrolysis zone ahead of the front, where the fuel undergoes thermal degradation, yielding a complex mixture of non-oxidized pyrolysis products. Some products have high boiling points and condense to form aerosols and tar like substances [6,25–28]. Their presence add to the complexity of the smoldering process as their roles are largely unknown. The high smoldering temperature of these liquid films could potentially enhance the spread of fire and, e.g., influence the transition of smoldering into flaming [29].

The propagating speed of a smoldering front influences the ability to control and contain a smoldering process. Speeds up to 5 mm/s have been observed when air is forced across smoldering filter paper [11,23]. Without forced air flow, but with increased fuel depth, typical smoldering velocities for various types of horizontally aligned solid fuel do not exceed 0.08 mm/s [1]. However, while the smoldering speed of liquid fuel in soil and sand have been measured (at up to 0.23 mm/s with forced air flow) [7,13], smoldering in thin liquid films is a very different mode of smoldering, which also requires a completely different experimental set-up.

To understand smoldering in liquid fuels, better knowledge of the driving mechanisms is required. Smoldering is typically an oxygen limited phenomenon [1,13], and for solid fuels the smoldering velocity is, e.g., highly sensitive to the depth of the fuel and the initial fuel temperature [30,31]. While several models exist for smoldering of solid fuels, this is less the case for liquid fuels [1]. Numerical models for smoldering liquid fuels in applications for soil remediation, have shown good agreement with experimental results [13,17]. Other numerical models [32] and models originating in material synthesis [33] could also contribute to understand the dynamics of smoldering liquids. However, these latter models seem to have been less exposed to experimental validation with liquid fuel, in particular liquid fuel that is directly exposed to air.

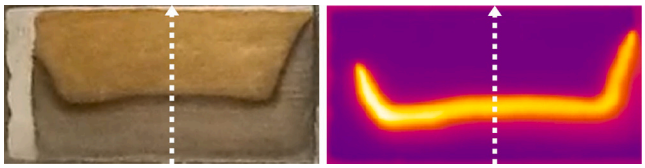

Fig. 2. Ordinary visual (left) and infrared thermographic (right) photos of the propagating smoldering front on a calcium silicate block. The temperature data analyzed in this paper is taken along the dashed center line. The propagating direction is indicated by the arrow head. Notice that the front propagation velocity is more than twice as fast at the peripheries of the front, but this does not affect the middle section.

The purpose of the current study is to provide better understanding of smoldering in liquid fuels based on experimental data. In particular, we study circumstances where the liquid fuel is dispersed on the surface of an inert porous substrate and where the oxidation occurs at very small depths. Key findings include the occurrence of smoldering in very thin layers of liquid fuel, replicating the combustion of condensed smoke on insulating building materials. The smoldering process happened at ambient temperatures just above room temperature, and could potentially mediate the fire spread. The dynamics of the smoldering process were quantified, and thermography revealed the existence of fluctuating double fronts that could be caused by unsteady-state conduction.

In Section 2 we describe the experimental set-up used to measure the propagating fronts, with experimental results and discussion presented in Section 3. The results include front velocities, peak temperatures and front widths, in addition to some interesting front instabilities. A first order theoretical model based on energy balance is presented and fitted to the observed data in Section 4. A demonstration experiment that illustrate how the thin fuel fronts can mediate the spread of fire in a fire safety context is presented in Section 5, followed by conclusions in Section 6.

2. Experimental set-up and procedure

The experimental setup has been developed to investigate how liquid fuel film thickness and initial fuel temperature influence the speed and temperature of smoldering fronts propagating across a porous, solid, and horizontally aligned surface.

2.1. Materials

Tar like deposits have previously been observed close to smoldering reactions in cotton and wood pellets [26–28]. In this paper we will investigate how this tar like material undergoes a smoldering process after being deposited on a porous surface. However, the observed tar from smoldering fires is unsuitable for controlled experiments. First, the tar deposit on a surface is not uniform, and the composition could vary between experiments. Second, it is time consuming to generate deposits from smoldering fires. In order to have a more uniform fuel, both in the chemical composition and as a deposit on a surface, a pyrolysis oil was used as a substitute for the deposits that are observed on surfaces during and after smoldering of cotton.

The employed fuel was a fast pyrolysis bio-oil (CAS No. 1207435-39-9, BTG-BTL, The Netherlands), which is also called wood derived bio-oil, wood oil or wood distillate. The oil is liquid condensate recovered by thermal treatment of pine wood at 450 – 600 °C at near atmospheric pressure or below, and in the absence of oxygen [34]. The pyrolysis oil exhibits a density of 1100 – 1300 kg/m^3 and contains

substantial amounts of water (~ 30 %), which evaporate when exposed to air.

Calcium silicate boards (Skamotec 225, Skamol, Denmark) was used as substrate in the experiments. The material has a micro-structure consisting of needle-shaped crystals and has low density (225 kg/m^3), high porosity (91 %), and low permeability (0.7 nPm to gases). Both the thermal conductivity (0.07 W/(m K)) and specific heat (0.84 kJ/(kg K)) are very low. These characteristics lead to small heat losses to the substrate and a large surface area per volume, where O_2 from the ambient air could react with fuel that had been applied to the substrate surface.

2.2. Experimental set-up

A sample consisted of a given amount of pyrolysis oil spread evenly over a 90 × 50 mm^2 area of a 3 mm thick calcium silicate board. Different amounts of oil was applied evenly to each block, and the oil did to a certain extent penetrate into the pores of the substrate. Small variations in film thickness over a single block was assumed to have little effect on the average front velocity u_{sm}.

The oil was allowed to dry for a minimum time interval (~ 24 h) between the time of application of fuel to substrate, and the time of ignition. Repeated weight measurements showed that a 24 h time interval was sufficient to ensure that most of the water in the pyrolysis oil had evaporated. Each sample was weighed before and after application of fuel in order to determine the area density ρ_A of the fuel film. The ignition temperature of the pyrolysis oil was determined experimentally to $T_{ign} \approx 350$ °C.

After drying and weight measurements, a thin strip of pyrolysis oil was applied onto the longest side (90 mm) of the 3 mm thin surfaces normal to the main surface. This strip served as a fuse with the intention to minimize the preheating of the fuel at the main face during the ignition process.

A schematic diagram of the experimental apparatus is presented in Fig. 1. The prepared samples (four samples were run in parallel) was placed in a tilted position on a hot plate (450 °C), such that only the bottom edge of the fuse layer touched the igniter (Fig. 1(a)). The fuse typically ignited after less than 30 s along the whole 90 mm length.

After ignition, the sample was moved to a second pre-heated hot plate, as shown in Fig. 1(b), where the front propagation continued. This hot plate served to heat the samples to a stable initial temperature. Preliminary experiments indicated that the initial temperature of the fuel T_0, and the substrate surface on which it was dispersed, had to exceed a critical threshold of ~ 50 °C to ensure stable self-sustaining smoldering fronts that did not self-extinguish before propagating across the whole main surface. The second hot-plate was set to a range of predetermined temperatures between 60 – 400 °C. The temperature of the fuel film on top of the substrate block quickly increased and stabilized at the initial fuel temperature T_0. The observed T_0 was 10 – 160 °C below the hot plate temperature, with larger differences for higher temperatures. The resulting temperature gradient from the hot plate through the substrate, could imply slightly higher initial fuel temperature deeper into the substrate compared to the surface temperature that was measured with the infrared camera. However, initially we assume that this only marginally affected the results since the applied fuel film was typically less than 10 % of the substrate block thickness. This assumption is discussed in more detail in Section 3.5.

The front propagation was captured by infrared camera (FLIR Thermacam SC500) at 240 × 320 display resolution, and digital temperature maps were collected every second with thermal emissivity set to 0.92. This type of indirect measurement of temperature enabled measurements of fast changes in temperature without affecting the experiment. Preliminary experiments showed that thermocouple measurements influenced the experiments by delaying the propagation of the fronts. Moreover, thermocouples had too large response time to capture the fast changes in temperature at the same level of detail as the infrared camera. As seen in Fig. 2, the analyzed temperature data were taken from the middle section of a 90 mm wide front. This part of the front was not affected by the boundary effects at the periphery of the front when the front propagated over a 50 mm distance.

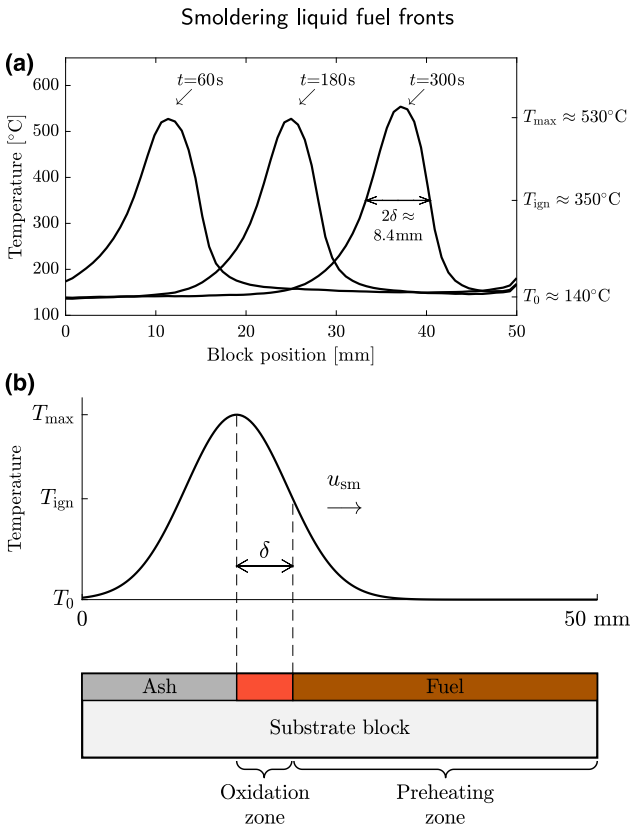

Fig. 3. (a) Temperature profiles of a propagating smoldering front with a 120 s time lapse between each profile. The hot plate temperature is 200 °C, the initial fuel temperature $T_0 \approx 140$ °C and the peak temperature $T_{max} \approx 530$ °C. The front width $\delta = 4.2$ mm is taken as half of the width of the temperature profile at ignition temperature $T_{ign} \approx 350$ °C. (b) Conceptual model of the smoldering process. Pyrolysis and heating of the fuel take place in the preheating zone, while smoldering occurs when the temperature exceeds the ignition temperature T_{ign}. The front width δ defines the width of the oxidation zone. After oxidation the temperatures fall and ash is left in the trail of the front. u_{sm} is the front propagation velocity, and the fuel film is characterized by the fuel area density ρ_A.

3. Experimental results with discussion

A total of 72 smoldering experiments were conducted. Here we first present how a smoldering front typically propagates. Thereafter, we quantify how the smoldering velocity u_{sm} and the front peak temperature T_{max} are governed by the fuel area density ρ_A and the initial fuel temperature T_0. The width δ of the smoldering front is also investigated, in addition to some instability phenomena, including double fronts.

3.1. A representative experiment

A representative experiment is shown in Fig. 2, where the smoldering front spreads across the substrate. Temperature data from a thermographic camera was used to develop temperature profiles of the propagating front like the ones in Fig. 3(a). The three instantaneous temperature profiles are at 120 s intervals, and the whole experiment lasted for 550 s from ignition to all fuel was consumed.

Notice the relatively stationary shape of the profiles and the rapid heating and cooling that take place before and after the front, respec-

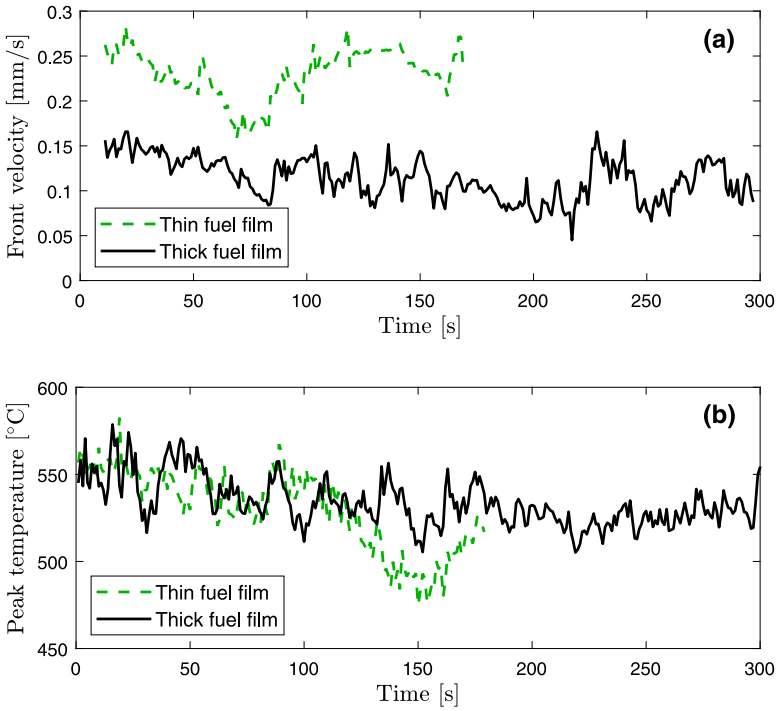

Fig. 4. (a) Smoldering front propagating velocity (moving average, 20 s intervals). The solid black line with average velocity $u_{sm} = 0.11$ mm/s is taken from the experiment in Fig. 3(a), where the film is relatively thick ($\rho_A = 0.19\,kg/m^2$). A thinner fuel film (dashed, green line, $\rho_A = 0.07\,kg/m^2$), with the same initial fuel temperature $T_0 \approx 140$ °C, gives higher average velocity, $u_{sm} = 0.22$ mm/s. (b) The front peak temperatures $T_{max} \approx 530$ °C are similar for the two experiments, and hence less dependent on the fuel area density ρ_A.

tively. In Fig. 3(a) the observed initial fuel temperature is $T_0 \approx 140$ °C,[1] and the peak temperature is $T_{max} \approx 530$ °C. The similar shapes of the profiles at different time steps indicate that the substrate and initial fuel temperature T_0 quickly stabilize according to the hot plate temperature.

The conceptual model in Fig. 3(b) shows how the oxidation process of the thin smoldering fronts starts at ignition temperature T_{ign}, and propagates through the fuel film with velocity u_{sm}, reaching a peak temperature T_{max}. The temperature decreases after oxidation is finished, and only small remnants of ash is left behind. The degree of pyrolysis reaction ahead of the front is assumed to be low, since the employed fuel had already undergone a controlled pyrolysis process at high temperatures by the producer of the pyrolysis oil.

The front could be visually observed as a distinct black curve (see Fig. 2), sometimes also appearing as glowing. Visual smoke did also accompany the front. Details of how the front width δ was defined and measured are found in Section 3.4. There were hardly any observed remains of, e.g., ash in the zone trailing the front. This was confirmed by weight observations of the substrate when stabilizing at ambient conditions after the end of experiments. This is in contrast to the observations of smoldering solids where significant amounts of ash and residual char are observed [28]. This could indicate that in our case all the fuel undergoes a complete combustion in the smoldering process. However, this cannot be concluded upon since the amount of unburned volatiles in the smoke is unknown, and the visual faint traces behind the front, undetectable by weight measurements, could be either ash or char (see Fig. 10).

Moving average front velocities are shown in Fig. 4(a) for the same experiment as in Fig. 3 (black, solid curve). Each data point is computed by measuring the distance the temperature peak is moving over 20 s intervals. Corresponding results are shown from another experiment with the same initial fuel temperature T_0, but thinner fuel film (green, dashed curve). Even though there are variations along the front velocity trajectory, the average velocity u_{sm} is higher when the fuel area density ρ_A is low (i.e., thin film).

Only the recorded data from the middle 60 % of the covered distance over the substrate block is used in the computation of the average smoldering velocity u_{sm}, the average peak temperature T_{max}, and the median front width δ. This is in order to avoid any boundary effects in the start and end phases of the front propagation across the substrate block. Such effects might arise from the time needed to stabilize the temperature of the substrate block after being placed on the hot plate. There could also be deviations in, e.g., oxygen supply and temperature near the edges compared to the middle sections of the substrate.

3.2. Smoldering front velocity

The velocity data from all the experiments are shown in Fig. 5. The data clearly demonstrates that the smoldering velocity u_{sm} is increasing with lower fuel area density ρ_A and higher initial fuel temperature T_0. The data are fitted to a first order approximation model (see Section 4) by non-linear regression, and the results confirm that both ρ_A and T_0 have high statistical significance in the data-fitted model estimate of the speed $\hat{u}_{sm}$ (see Appendix B).

As with solid fuels [9], it follows naturally that the front velocity is inversely proportional to the fuel area density ρ_A since it takes less oxygen and time to consume a thin fuel film compared with a thick fuel film. The underlying assumption is that the smoldering process is limited by the supply of oxygen and that the supply of oxygen to the reaction zone is relatively similar for experiments with equal initial fuel temperature T_0. Even though a process where virtually all the fuel is consumed by combustion could be fuel limited, there are several observations that in this case corroborate the assumption of an oxygen limited process. First, the observations in Figs. 5 and 12 indicate that the velocity is inversely proportional to the fuel density as in other oxygen limited smoldering experiments [23]. With a fuel limited process, one would not expect the smoldering velocity to decrease with increased fuel thickness. Second, the velocity was observed to be

[1] The initial fuel temperature T_0 is defined as the median temperature at the second 10 mm stretch of the covered distance over the substrate block, after smoldering is finished.

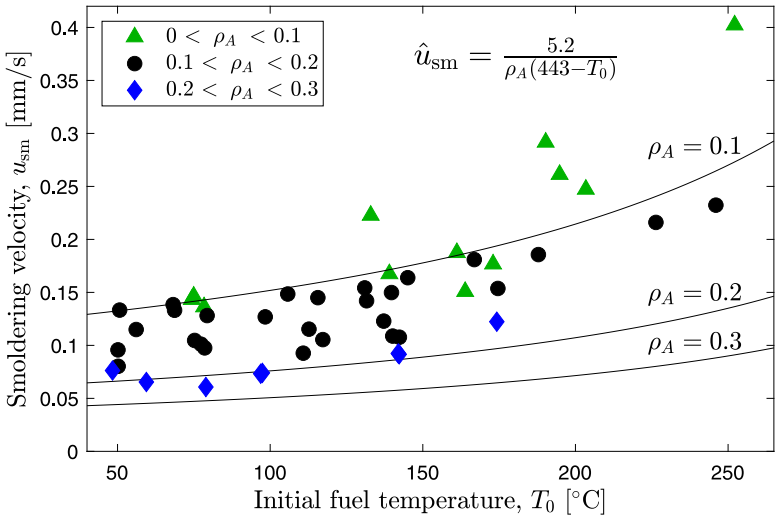

Fig. 5. The smoldering propagating velocity u_{sm} is clearly increasing as a function of higher initial fuel temperature T_0 and lower fuel area density ρ_A (indicated by different colored marker symbols). Each data point is the average of the middle section of a moving average trajectory like those shown in Fig. 4(a). The data-fitted model velocity $\hat{u}_{\mathrm{sm}}$ is shown for three different values of ρ_A (solid lines). $\hat{u}_{\mathrm{sm}}$ is found by non-linear regression based on a simplified energy balance model (see Section 4). (For interpretation of the references to color in this figure legend, the reader is referred to the web version of this article.)

higher at the peripheries of the front (see Fig. 2), and since the initial fuel temperatures were similar to elsewhere on the substrate, the most likely reason seems to be that there was more oxygen available at the peripheries of the front.

That the velocity increase with higher initial fuel temperature T_0, could be related to the fact that it takes less time to heat the fuel to ignition temperature T_{ign}. Moreover, the front width is shown to increase with higher initial temperatures (see Section 3.4 below). Hence, the reaction surface area that is in direct contact with air is larger, which allows for a higher total rate of O_2 supply to the smoldering reaction. Higher peak temperatures T_{max} (see Section 3.3 below) could potentially also increase the oxygen supply through increased buoyancy of the surrounding air. Accordingly, the smoldering propagation is faster with higher initial fuel temperature. This heuristic reasoning is also reflected by the quantitative model in Section 4, which is based on energy balance.

For solid fuels, there are also other factors that affect the smoldering velocity, e.g., moisture and inert content, particle size, heat transfer coefficients, thermal conductivity, oxygen mass fraction, and heat loss to surroundings [25,31,35–37]. Whether these factors also could influence the smoldering velocity of thin liquid fuel films is not investigated in this paper.

3.3. Peak temperature

The smoldering peak temperature T_{max} for the experiments is shown in Fig. 6. T_{max} is increasing with higher initial fuel temperature T_0. A first approximation gives a 0.43 °C rise in peak temperature T_{max} for each 1 °C increase in initial fuel temperature T_0. This means that the rise in T_{max} is less than the increase in T_0. As noted above, a balance seems to be established where the temperature increase results in both increased heat loss to the ambient air and faster front propagation u_{sm} due to higher supply of O_2 to the reaction.

The fuel area density ρ_A seems to have little influence on the peak temperature T_{max} in Fig. 6, and ρ_A is not statistically significant in the linear regression model (see Appendix B). This is also indicated by the two experiments in Fig. 4(b) where the peak temperatures are quite similar for both the thin and the thick fuel films (with T_0 fixed).

3.4. Front width

As indicated in Fig. 3(b), the front width is defined to be half of the width of the temperature profiles at the ignition temperature $T_{\mathrm{ign}} \approx 350$ °C. For each experiment the median front width δ during the front propagation (across the middle 60% section of the block) is computed and shown in Fig. 7. The front widths are increasing with higher initial fuel temperature T_0 and — to a lesser extent — also increasing with higher fuel area density ρ_A. In a linear regression model for δ based on the experimental data, both T_0 and ρ_A are highly statistically significant.

An increase in front width δ is also expected when T_0 increases. If the shape of the temperature profile is maintained, the area with temperatures above T_{ign} will increase and accordingly also the front width δ. The front width δ also increases with increased fuel area density ρ_A. Thicker film reduces the front velocity, and this could increase the heat transfer by convection ahead of the front which in turn enables the smoldering to take place at a wider area.

3.5. Double fronts

When the front widths in Fig. 7 exceeded 6 mm, the fronts usually entered a mode with *double fronts* where the temperature profiles took the shape of two peaks in close succession. A typical example is shown in Fig. 8. The location of the highest temperature peak is fluctuating back and forth between the leading and the trailing peak. In Fig. 8 only a few snapshots are shown, but such fluctuations could take place more than 10 times during the propagation across the substrate.

The experimental data in Fig. 9 demonstrates that the likelihood of observing a double front is increasing with higher initial fuel temperature T_0 and higher fuel area density ρ_A, following a similar trend as the front widths in Fig. 7. The estimated transition region is indicated in the figure. Above the transition region it is very likely that a new experiment will result in a double front. Conversely, it is very unlikely to observe a double front below the region. The estimated region is obtained by a logistic regression model (see, e.g., [38]) which shows high statistical significance for both T_0 and ρ_A (see Appendix B).

The double fronts with splitting of the front into two peaks could be due to insufficient supply of oxygen to the middle section of the reaction zone when the front width δ exceeds a certain limit of approximately 6 mm in Fig. 7. The leading part of the front is likely to be supplied with oxygen from incoming air towards the front, while the

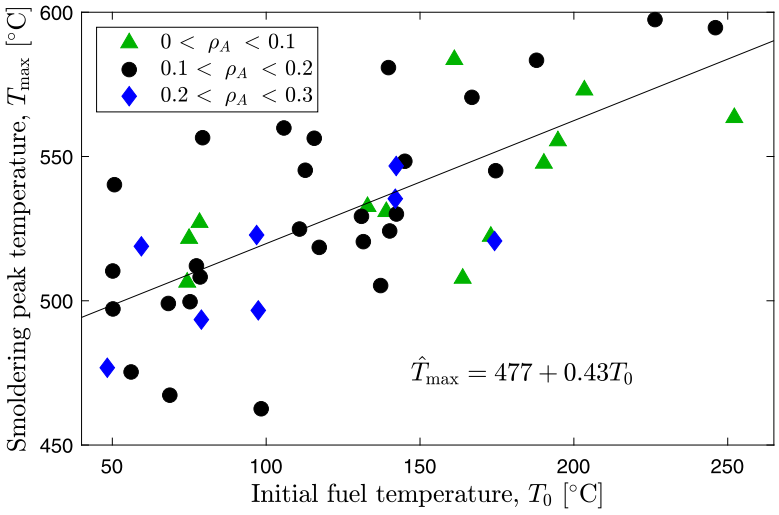

Fig. 6. The front peak temperature $T_{\max}$ is increasing as a function of higher initial fuel temperature T_0. However, the data does not indicate that $T_{\max}$ depends on the fuel area density ρ_A. The data-fitted peak temperature $\hat{T}_{\max}$ is based on simple linear regression (solid line).

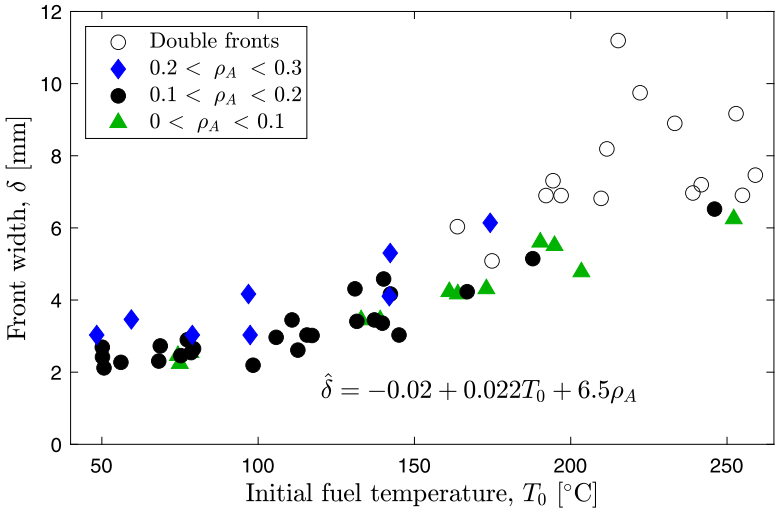

Fig. 7. The front width δ is increasing as a function of higher initial fuel temperature T_0. There is also a slight increase with higher fuel area density ρ_A. When the front width exceeds a certain threshold, two peaks in close succession can be observed in the temperature profiles (double fronts, Fig. 8). The data-fitted front width $\hat{\delta}$ is based on simple linear regression of the observed data without double fronts.

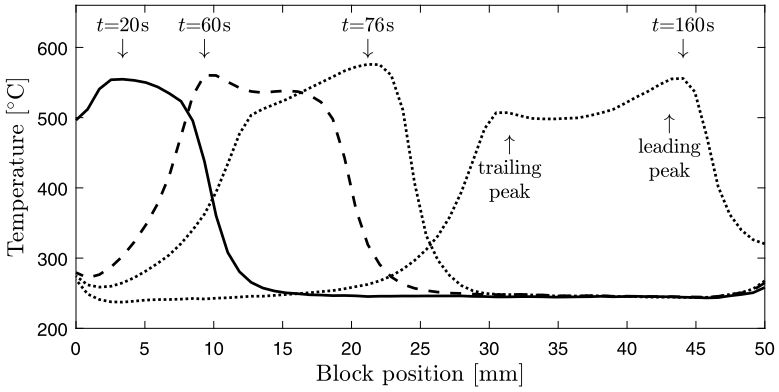

Fig. 8. Temperature profiles of a propagating double front at different time steps t. From the start, there is one peak (solid curve), but after a while two peaks emerge. The location of the highest peak is fluctuating back and forth between the trailing peak (dashed curves) and the leading peak (dotted curves). The experiment was performed with both high initial fuel temperature (T_0 = 233 °C) and high fuel area density (ρ_A = 0.16 kg/m^2). An animation of the propagating temperature profile is found in the Supplemental Data available online.

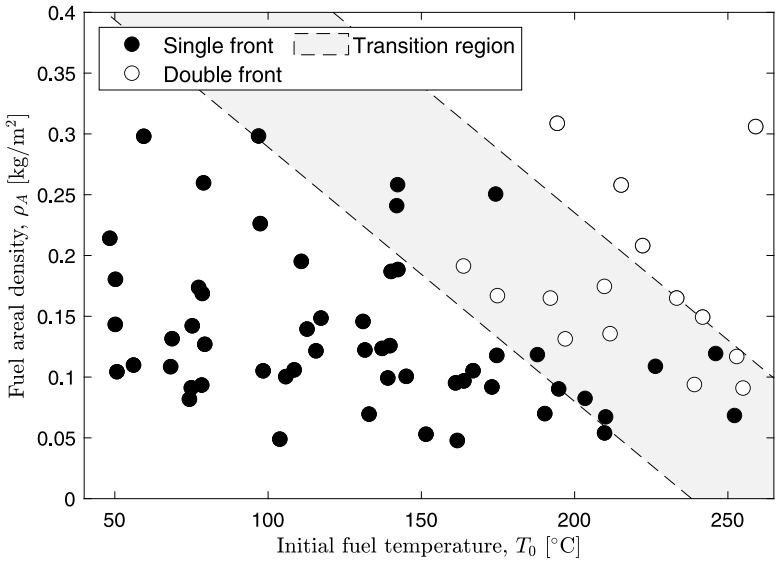

Fig. 9. Double fronts are more likely to occur with high initial fuel temperatures T_0, and high fuel area density ρ_A. Based on a simple logistic linear regression model, the likelihood of double front is more than 90 % on the upper side of the transition region and less than 10 % below the region.

trailing part of the front consumes the remaining fuel as it is supplied with oxygen from the backside of the front. Moreover, thick fuel films would seep deeper into the substrate, and the occurrence of double fronts might be enhanced by the time it takes for oxygen to reach the deeper layers of the fuel.

The emergence of the fluctuating double fronts could also be induced by possible unsteady-state conduction. As mentioned in Section 2.2, we initially assumed that the temperature difference between the hot-plate and the substrate surface only marginally affected the experiments. This can be compared to the model assumptions for a semi-infinite slab with thickness L, where the process on one side of the slab is assumed not to be affected by the temperature at the other side of the slab during the initial stage. However, the substrate is relatively thin ($L \approx 3$ mm), and this assumption can be challenged, in particular when the temperature gradient through the substrate is large.

The characteristic length of a process in a semi-infinite slab model is typically defined by $l_c = \sqrt{\alpha t_c}$, where $\alpha = k_s/(\rho_s c_{p,s}) = 3.7\times10^{-7}$ m^2/s is the thermal diffusivity of the substrate (see Section 2.1), and $t_c = \delta/u_{\mathrm{sm}}$ is taken as the characteristic time of the moving temperature profile. The assumptions for the semi-infinite slab model are likely to hold if $2l_c < L$ [39], i.e.,

$$2l_c = 2\sqrt{\frac{\alpha\delta}{u_{\mathrm{sm}}}} < L. \tag{1}$$

However, for the experiments where double fronts were observed, observed values of $2l_c$ are in the range of 5.8 – 9.1 mm, which is well above $L \approx 3$ mm. For the experiments without detectable double fronts, most values of $2l_c$ are less than 7 mm, while a few are also higher. This indicates that there could be an increasing unsteady-state effect on the smoldering process when the temperature gradient through the substrate is high (i.e., high hot-plate temperature), which in turn might contribute to the formation of a second peak in the temperature profile. More experiments and more detailed modeling are required to evaluate this hypothesis.

Some explanation of the observed fluctuations between the leading and the trailing peak in Fig. 8, could possibly be found in related pulsating combustion phenomena. Two fluctuating fronts with opposite phase are observed experimentally in downward flame spread over thick paper [40], while conditions for oscillatory behavior can be derived from mathematical combustion models [19,41]. The fluctuations could also be related to the patterns of visible bands of ash, which are sometimes observed at quite regular intervals behind the smoldering fronts[2] (see Fig. 10(a)). Further studies of such potential relationships are not expanded upon in this paper.

Fig. 10. (a) The visual pattern of the ashes after the smoldering front could be related to the fluctuations of the two-peaked temperature profiles. The picture is taken from the same experiment as in Fig. 8. (b) The fingering pattern of a dying front at low temperature T_0 and low fuel area density ρ_A.

Notice that experiments exhibiting a double front have been excluded from the analysis of smoldering velocity u_{sm} and smoldering peak temperature $T_{\max}$ in Figs. 5 and 6, respectively. As outlined above, smoldering with double fronts can be considered a different mode of smoldering and must therefore be treated separately.

3.6. Fingering instability

While the double front instability was observed for high fuel temperatures and high fuel area densities, another type of instability were observed for the opposite settings. For sufficiently low initial fuel temperatures and low fuel area densities, preliminary experiments demonstrated smoldering fronts propagating in unstable fingering patterns that eventually self-extinguished before all the fuel had been consumed. A typical fingering pattern after a complex series of front propagations is shown in Fig. 10(b). The lateral width of the observed fingering fronts is diminishing at varying rates. The heat loss seems to be exceeding the rate of heat generation at the peripheries of the front, while the middle of the front is able to proceed due to less heat loss.

[2] Notice that similar patterns can also be observed after some of the experiments without detectable double fronts.

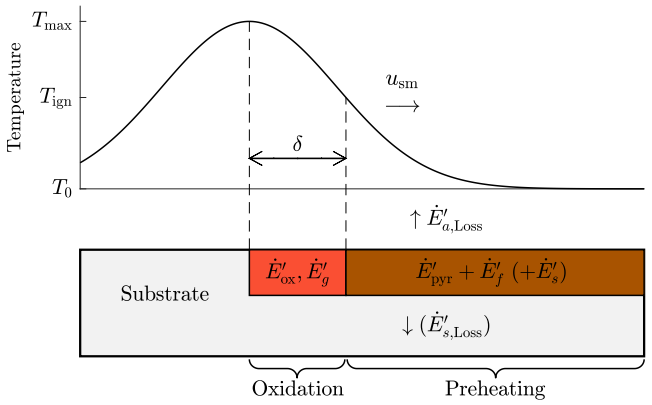

Fig. 11. Schematic of the energy balance of a stationary smoldering front. Fuel and substrate is preheated to the ignition temperature T_{ign} in the preheat zone. The volatiles from the reaction are heated further in the smoldering zone. Heat loss is mainly to the air which is transported by buoyancy.

4. Simplified model for smoldering velocity u_{sm}

A simple analytical model for the prediction of the propagating velocity u_{sm} of a smoldering front was presented by Dosanjh et al. [42]. The model is based on energy balance, and has been further developed by others. Both opposed and forward smoldering have been examined, and earth conditions were compared with micro-gravity experiments using such models [43–46]. For forward smoldering, the model has also been used to determine the critical size of a block of polyurethane foam for self-sustained smoldering [47]. A similar model has been used to predict the front speed based on the total supply of O_2 [11,23].

Adapting the model of Dosanjh et al. [42] to the current experiments, a model for the smoldering velocity in thin layers of liquid fuel has been developed. The model is based on a steady-state energy balance in the control volume consisting of the oxidation and preheating zones illustrated in Fig. 11. As with other type of smoldering [13], the O_2-supply is assumed to be the main limiting mechanism (see Section 3.2). Even though an ample supply of oxygen is available from the surrounding air, the thickness and depth of the fuel film are large in stoichiometric terms. The smoldering front is chosen as the frame of reference for the control volume. Hence, it is moving at the stationary speed u_{sm}.

The steady state energy balance is based on the assumption that the generated heat ($\dot{E}'_{ox}$ generated by the exothermic reaction in the smoldering zone) equals the heat transferred to or lost to the pre-heating zone, the smoldering zone and the surroundings.

$$\begin{aligned}\dot{E}'_{ox} &= \dot{E}'_{pyr} + \dot{E}'_f + \dot{E}'_s && \text{(Pre-heat zone)}\\ &\quad + \dot{E}'_g && \text{(Smoldering zone)}\\ &\quad + \dot{E}'_{a,Loss} + \dot{E}'_{s,Loss} && \text{(Heat loss)}\\ &\approx \dot{E}'_{pyr} + \dot{E}'_f + \dot{E}'_g + \dot{E}'_{a,Loss}. && (2)\end{aligned}$$

Here, heating of the substrate $\dot{E}'_s$ and heat loss to the substrate beneath the fuel film $\dot{E}'_{s,Loss}$ are considered negligible relative to the other terms, due to the low specific heat and low thermal conductivity of the substrate. Each of the terms in Eq. (2) will be detailed in the following, and for nomenclature, see Appendix A.

The generation of heat is limited by the oxygen supply, which is assumed to be governed mainly by the buoyant air flow u_b above the smoldering zone, such that

$$\dot{E}'_{ox} = \dot{m}'_{O_2} Q_{ox} \approx u_b y_{O_2} h \rho_a Q_{ox}. \quad (3)$$

We assume that the amount of oxygen that is consumed in the smoldering zone is proportional both to the mass fraction of oxygen y_{O_2} and the thickness of the boundary layer of the horizontal influx of air [39]. The latter is represented by an effective height h from which the air supplies the oxidation zone with O_2. The air is subsequently heated and rises by buoyancy. The buoyant air flow velocity is roughly given by $u_b \propto (T_{max} - T_a)$, but will vary with the temperature profile along the surface, and an exact expression is not readily available. The effective height h of the incoming air stream also takes into account the effective area of fuel that is in contact with the air.

In order to ignite the fuel, the fuel must be heated to a sufficiently high temperature. In addition, remaining pyrolysis and vaporization of any remaining water must take place. The main reactions in the pre-heat zone are

$$\begin{aligned}\dot{E}'_f &= u_{sm} \rho_A c_{p,f} (T_{ign} - T_0)\\ \dot{E}'_{pyr} &= u_{sm} \rho_A Q_{pyr}.\end{aligned} \quad (4)$$

The fuel is heated from its initial temperature T_0 to ignition temperature T_{ign}. Q_{pyr} is the heat required for remaining pyrolysis of the fuel and also vaporization of any remaining water content.

The main heat sink in the smoldering zone is heating of the volatile combustion products from ignition temperature T_{ign} to peak temperature T_{max},

$$\dot{E}'_g = u_{sm} \rho_A c_{p,g} (T_{max} - T_{ign}). \quad (5)$$

The heat loss to the surroundings is assumed to be mainly by natural convection, and mainly above the smoldering zone where the temperature difference between sample and ambient air is at its largest. Incoming air is heated at a rate governed by the buoyant air flow velocity, u_b, such that:

$$\dot{E}'_{a,Loss} \propto u_b \rho_a c_{p,a} (T_{max} - T_a). \quad (6)$$

However, notice that the loss rate varies along the temperature profile, and that a precise estimate is hard to achieve. As mentioned above, there is also some heat loss into the substrate below the smoldering zone, but this is considered to be marginal in our application.

It is also assumed that the heat transfer in the direction of the burned fuel is negligible. As indicated in Fig. 11, the temperature is assumed to be quite constant at this surface of the control volume, resulting in minimal conductive heat loss. Moreover, the area of this surface is small, so convective and radiant heat losses are also assumed to be small.

The first three terms on the right-hand side of Eq. (2) are governed by the smoldering speed u_{sm}. Inserting Eqs. (3)–(5) into Eq. (2), the smoldering speed can now be found by solving for u_{sm}, such that

$$u_{sm} \approx \frac{\dot{m}'_{O_2} Q_{ox} - \dot{E}'_{a,Loss}}{\rho_A [c_{p,f} (T_{ign} - T_0) + c_{p,g} (T_{max} - T_{ign}) + Q_{pyr}]} \quad (7)$$

$$\approx \frac{\hat{\alpha}_1}{\rho_A (\hat{\alpha}_2 - T_0)} \equiv \hat{u}_{sm}. \quad (8)$$

In Eq. (8), $\hat{u}_{sm}$ is a simplified data-fitted model for u_{sm}, and the unknown constants $\hat{\alpha}_1$ and $\hat{\alpha}_2$ are fitted to the experimental data by non-linear regression. The data-fitted values for $\hat{\alpha}_1$ and $\hat{\alpha}_2$ are presented in Figs. 5 and 12. We have assumed that the numerator in Eq. (7) is approximately constant since both $\dot{m}'_{O_2}$ and $\dot{E}'_{a,Loss}$ are slowly increasing with T_0. Moreover, in the present range of temperatures, any increases in the two terms will to some degree cancel each other out, and the numerator is therefore represented by the constant $\hat{\alpha}_1$. In the denominator, the representation by $\hat{\alpha}_2$ is based on the observed linear relationship between T_{max} and T_0 in Fig. 6. In Fig. 12 the estimate $\hat{u}_{sm}$ is shown to correspond very well with the experimental data.

For the experiments where double fronts were observed, the front width δ was generally larger than for the other experiments (see Fig. 7). Hence, with double fronts the smoldering takes place at a significantly larger surface area that is directly exposed to air. This enables increased supply of oxygen to the reaction front, and might explain why the observed velocities in Fig. 12 in general are higher for these experiments.

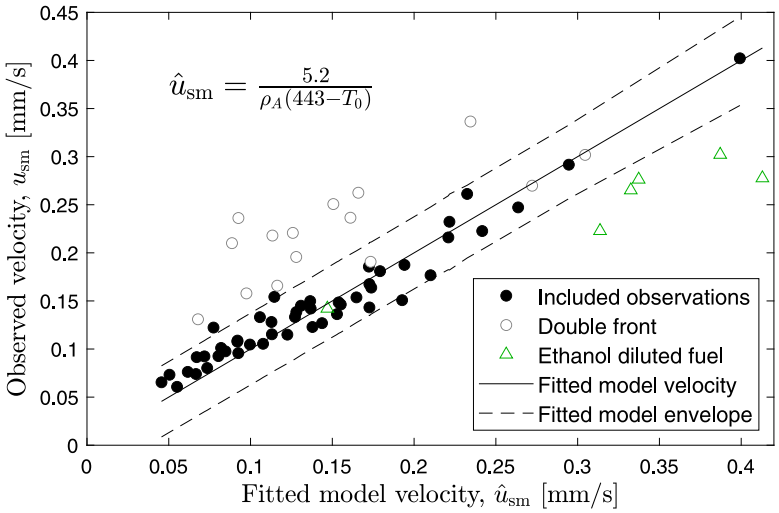

Fig. 12. The simplified data-fitted model of the smoldering velocity, $\hat{u}_{\mathrm{sm}}$ in Eq. (8), has a strong fit to the experimental data. However, observations deviating from model assumptions show other behaviors: double fronts have higher velocities[3]due to better O_2 supply, while fuel diluted with ethanol could be situated deeper into the substrate where O_2 supply is less available (see main text for description of these additional experiments).

I.e., the velocities are higher than predicted by the model in Eq. (8), where data from double front experiments are excluded from the model fit.

Some additional experiments were conducted with ethanol diluted fuel in order to be able to apply even thinner fuel films (as the ethanol quickly vaporized after application). As indicated in Fig. 12, all those experiments showed lower velocity than the data-fitted model velocity $\hat{u}_{\mathrm{sm}}$ in Eq. (8). The reason could be twofold. First, the fuel could have seeped deeper into the substrate and then become less available for oxygen. Second, one could anticipate that the thin films could be close to an unstable regime where the heat loss in the nominator in Eq. (7) (including heat loss to the substrate $\dot{E}'_{s,\mathrm{Loss}}$) is approaching the amount of heat generated.

5. Demonstration experiment — fire spread

Finally, we present a demonstration experiment that is potentially highly relevant in terms of understanding how smoldering in condensed smoke films could affect the spread of fire. Fig. 13 shows that smoldering fronts in thin layers of liquid fuel also can effectively mediate the spread of fire between a heat source and other types of fuel. Before being placed on the hot plate at 400 °C, the left calcium silicate block in Fig. 13 was first exposed to the smoke from smoldering cotton. Volatiles in the smoke condensed as a thin film on the block. This film was ignited by the hot plate, and a smoldering front propagated upwards and ignited a virgin cotton sample located 4 cm above the surface. The cotton sample was subsequently almost completely consumed by smoldering. Another cotton sample located at the same height, at a block (right in Fig. 13) without condensed deposits, was virtually unaffected by the heat produced by the hot plate. The two different scenarios illustrate how condensed liquids may affect spread of smoldering fire, and how this can affect fire safety when smoldering is occurring.

6. Conclusion

In this article we have presented results from experiments of smoldering in thin liquid fuel films. The experiments demonstrate that the minimal liquid fuel film thickness[4] to obtain self-sustaining fronts is less than 0.1 mm on porous media with low heat capacity. This is much less than the critical thickness for solid fuels, like dust, where the minimal thickness is reported to be several centimeters [31]. Even though the heat loss to the surroundings was relatively large in our experiments, this seemed to be counterbalanced by efficient insulation in the substrate below and high supply of oxygen from the air above. These properties seem to be even more crucial for the self-sustaining smoldering of thin films than for the smoldering of solids [7].

The high observed propagating velocity u_{sm} of the smoldering fronts that were measured up to 0.4 mm/s, are surprising. This is faster than previously observed for solid fuels at similar environmental conditions but with thicker layer of fuels [1]. The smoldering velocity was shown to increase with increasing initial fuel temperature and fuel area density. The findings are consistent with a simple model based on energy balance where oxygen supply is the main limiting mechanism.

Infrared thermography enabled detailed observations of the temperature characteristics of the propagating fronts with high resolution both in time and space. By using temperature data from the infrared camera, it could also be empirically shown to what extent the peak temperatures and front widths depended on the initial parameters. The findings were quantitatively corroborated by statistical analyses that highlighted correlations that to some degree were obscured by the relatively large natural variations both within and across experiments.

In addition to the large number of experiments that were conducted at conditions close to steady state, we have also described two different instability phenomena. Experiments with pulsating double fronts seem to have entered a mode that increase the oxygen supply, which is the main limiting factor of the steady state smoldering velocity. Unsteady-state conduction could be a cause for this phenomenon, but more experiments and detailed modeling should be performed to confirm this hypothesis. Another mode, with heat loss as a main limiting mechanism, was observed in the form of fingering patterns. These were generated by transient dying fronts in thin films at low initial fuel temperatures.

The quasi-2D feature of the thin films can make the experimental set-up an interesting candidate for experiments where other combustion characteristics or dynamics are to be investigated. Another experimental setting that should be considered is vertical alignment of the fuel

[3] For the experiments with double front, the velocity was calculated by tracking the mid-point between the two positions where the temperature profile equaled $T_0 = 350$ °C (estimated ignition temperature).

[4] A fuel area density of $\rho_A = 0.05\,\mathrm{kg/m^2}$ corresponds to an approximate film thickness of 0.04 mm.

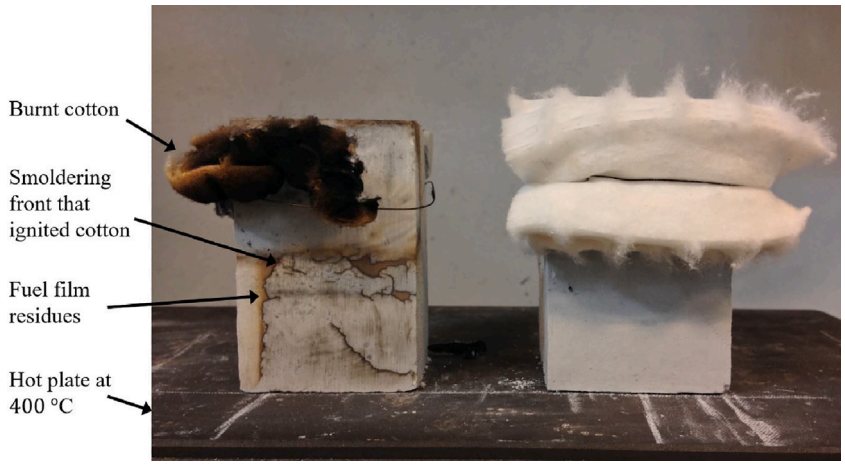

Fig. 13. Demonstration experiment. *Left block:* A thin fuel film covering the bottom half of the substrate block was ignited from below by the hot plate (400 °C). A smoldering front propagated upwards and finally ignited a cotton sample placed 4 cm above the hot plate. The picture is taken after the cotton has been almost completely consumed by smoldering. Before heating, the fuel film on the block was generated by exposing the front face to smoke from smoldering cotton. The smoke condensed on the substrate as a film. *Right block:* The block has not been exposed to smoke before the experiment, and the attached cotton is virtually unaffected by the heat from the hot plate.

film. This could be closer to conditions during real fire scenarios where smoke often condense on vertical walls. Pilot experiments indicate that the smoldering velocity is higher than with the horizontally aligned surfaces considered in this paper. The oxygen supply is higher under such conditions since the buoyancy driven air velocities are higher along vertical walls.

Considering the main implications for fire safety, the demonstration in Fig. 13 reveals that the smoldering fronts in liquid fuel deposits can mediate the spread of fire. Similar smoldering fronts have also been observed by the authors on some types of insulating mineral wool that share many of the same characteristics with calcium silicate. Calcium silicate boards are commonly used as building boards for fireplace enclosures. It should in particular be emphasized that the surface of such porous insulating materials should be sealed to suppress smoldering as noted by Drysdale [25]. Whether the condensed smoke and smoldering fronts also play a role in the transition of smoldering into flaming is an area that should be set up for further investigation.

CRediT authorship contribution statement

Sveinung Erland: Conceptualization, Data curation, Formal analysis, Investigation, Methodology, Project administration, Resources; Software, Supervision, Validation, Visualization, Writing – original draft, Writing – review & editing. **Runald Meyer:** Conceptualization, Data curation, Formal analysis, Investigation, Methodology, Validation, Writing – original draft, Writing – review & editing. **Bjarne C. Hagen:** Conceptualization, Funding acquisition, Investigation, Methodology, Writing – review & editing.

Declaration of competing interest

The authors declare that they have no known competing financial interests or personal relationships that could have appeared to influence the work reported in this paper.

Acknowledgments

This work was supported by the Research Council of Norway [grant number 238329 (EMRIS)]. Special thanks to Vidar Frette for valuable comments on the work.

Appendix A. Nomenclature

Latin letters	
c_p	Specific heat capacity, J/(kg K)
$\dot{E}'$	Energy rate, W/m
h	Effective height, m
k	Thermal conductivity, W/(m K)
L	Substrate thickness, m
l_c	Characteristic length, m
$\dot{m}'_{O_2}$	Mass rate of O_2, kg/(m s)
Q_{pyr}	Heat of pyrolysis, J/kg
Q_{ox}	Exothermic heat, J/kg[O_2]
T	Temperature, °C
T_0	Initial fuel temperature, °C
T_{ign}	Fuel ignition temperature, °C
T_{max}	Smoldering peak temperature, °C
t	Time, s
t_c	Characteristic time, s
u_b	Buoyant velocity of gas, m/s
u_{sm}	Smoldering propagation velocity, m/s
$\hat{u}_{sm}$	Estimated propagation velocity, m/s
y_{O_2}	Fraction of O_2 in air
Greek Symbols	
α	Thermal diffusivity, m^2/s
δ	Front width, m
ρ	Density, kg/m^3
ρ_A	Fuel area density, kg/m^2
Subscripts	
a	Ambient air
f	Fuel
g	Volatiles
s	Substrate
ign	Ignition
ox	Oxidation
pyr	Pyrolysis
sm	Smoldering

Appendix B. Statistical analysis

Details from the non-linear and linear regression analyses referred to in Section 3 are presented in Tables 2–5. N is the number of observations. R^2 is the proportion of the variance in the dependent variable that is explained by the model. The observed F-test statistic

Table 2
Estimated coefficients from the non-linear regression model of the smoldering velocity $\hat{u}_{sm} = \hat{\alpha}_1/[\rho_A(\hat{\alpha}_2 - T_0)]$.

	$\hat{\alpha}_i$	Std.dev.$[\hat{\alpha}_i]$	p-value
α_1	5.21	0.40	5.4×10^{-17}
α_2	442.8	20.0	3.7×10^{-26}
$N = 48,\ R^2 = 0.921,\ F = 1770,\ p = 3.0 \times 10^{-44}$.			

Table 3
Estimated coefficients from the linear regression model of the peak temperature $\hat{T}_{max} = \hat{\alpha}_0 + \hat{\alpha}_1 T_0$. An additional term $\hat{\alpha}_2 \rho_A$ did not prove to be significantly different from zero (p-value: 0.47).

	$\hat{\alpha}_i$	Std.dev.$[\hat{\alpha}_i]$	p-value
α_0	477.2	8.6	8.8×10^{-44}
α_1	0.426	0.064	2.7×10^{-8}
$N = 48,\ R^2 = 0.49,\ F = 44.7,\ p = 2.7 \times 10^{-8}$.			

Table 4
Estimated coefficients from the linear regression model of the front width $\hat{\delta} = \hat{\alpha}_0 + \hat{\alpha}_1 T_0 + \hat{\alpha}_2 \rho_A$.

	$\hat{\alpha}_i$	Std.dev.$[\hat{\alpha}_i]$	p-value
α_0	−0.02	0.25	0.9
α_1	0.022	0.0012	3.4×10^{-21}
α_2	6.45	1.06	2.9×10^{-7}
$N = 46,\ R^2 = 0.88,\ F = 154,\ p = 2.5 \times 10^{-20}$.			

Table 5
Estimated coefficients from the logistic regression model where Prob{Double front$|T_0, \rho_A\} = e^{\hat{\alpha}_0 + \hat{\alpha}_1 T_0 + \hat{\alpha}_2 \rho_A}/(1 + e^{\hat{\alpha}_0 + \hat{\alpha}_1 T_0 + \hat{\alpha}_2 \rho_A})$.

	$\hat{\alpha}_i$	Std.dev.$[\hat{\alpha}_i]$	p-value
α_0	−16.3	4.6	4.0×10^{-4}
α_1	0.059	0.017	4.0×10^{-4}
α_2	28.3	10.8	8.7×10^{-3}
$N = 69,\ \chi^2 = 44.7,\ p = 2.7 \times 10^{-10}$.			

is assumed to be approximately Fisher distributed and is accompanied by a p-value that estimates the probability of observing an F-value at least as large as the observed one, given that the true parameters $\alpha_{i>0}$ are zero. Low p-values indicate that the model parameters are truly different from zero. Parameters are usually called significant if the p-value is less than a chosen significance level (here: 0.05). For each individual parameter, T-test statistics have been used to obtain the p-values.

Appendix C. Supplementary data

Supplementary material related to this article can be found online at https://doi.org/10.1016/j.firesaf.2022.103645.

References

[1] G. Rein, Smoldering combustion, in: SFPE Handbook of Fire Protection Engineering, 5th Ed., Springer New York, New York, NY, 2016, pp. 581–603, http://dx.doi.org/10.1007/978-1-4939-2565-0_19, chapter 19.

[2] J.L. Torero, J.I. Gerhard, M.F. Martins, M.A. Zanoni, T.L. Rashwan, J.K. Brown, Processes defining smouldering combustion: Integrated review and synthesis, Prog. Energy Combust. Sci. 81 (2020) 100869, http://dx.doi.org/10.1016/j.pecs.2020.100869.

[3] D. Drysdale, Ignition of liquids, in: SFPE Handbook of Fire Protection Engineering, 5th Ed., Springer, New York, 2016, pp. 554–580, http://dx.doi.org/10.1007/978-1-4939-2565-0_18, chapter 18.

[4] P. Bowes, Fires in oil soaked lagging. BRE current paper, Build. Res. Establishment (1974).

[5] A.C. McIntosh, M. Bains, W. Crocombe, J.F. Griffiths, Autoignition of combustible fluids in porous insulation materials, Combust. Flame 99 (1994) 541–550, http://dx.doi.org/10.1016/0010-2180(94)90047-7.

[6] M.F. Martins, S. Salvador, J.F. Thovert, G. Debenest, Co-current combustion of oil shale – part 2: Structure of the combustion front, Fuel 89 (2010) 133–143, http://dx.doi.org/10.1016/j.fuel.2009.06.040.

[7] P. Pironi, C. Switzer, G. Rein, A. Fuentes, J.I. Gerhard, J.L. Torero, Small-scale forward smouldering experiments for remediation of coal tar in inert media, Proc. Combust. Inst. 32 (2009) 1957–1964, http://dx.doi.org/10.1016/j.proci.2008.06.184.

[8] A. Shah, R. Fishwick, J. Wood, G. Leeke, S. Rigby, M. Greaves, A review of novel techniques for heavy oil and bitumen extraction and upgrading, Energy Environ. Sci. 3 (2010) 700–714, http://dx.doi.org/10.1039/B918960B.

[9] D.S. Kellogg, B.E. Waymack, D.D. Mcrae, R.W. Dwyer, Smolder rates of thin cellulosic materials, J. Fire Sci. 15 (1997) 390–403, http://dx.doi.org/10.1177/073490419701500504.

[10] S. Olson, H. Baum, T. Kashiwagi, Finger-like smoldering over thin cellulosic sheets in microgravity, Symp. Int. Combust. 27 (1998) 2525–2533, http://dx.doi.org/10.1016/S0082-0784(98)80104-5.

[11] O. Zik, Z. Olami, E. Moses, Fingering instability in combustion, Phys. Rev. Lett. 81 (1998) 3868–3871, http://dx.doi.org/10.1103/PhysRevLett.81.3868.

[12] J. Brindley, J.F. Griffiths, A.C. McIntosh, J. Zhang, The role of liquid-fuel vaporization and oxygen diffusion in lagging fires, Symp. Int. Combust. 27 (1998) 2775–2782, http://dx.doi.org/10.1016/S0082-0784(98)80134-3.

[13] T. Hasan, J.I. Gerhard, R. Hadden, G. Rein, Self-sustaining smouldering combustion of coal tar for the remediation of contaminated sand: Two-dimensional experiments and computational simulations, Fuel 150 (2015) 288–297, http://dx.doi.org/10.1016/j.fuel.2015.02.014.

[14] M. Salman, J.I. Gerhard, D.W. Major, P. Pironi, R. Hadden, Remediation of trichloroethylene-contaminated soils by star technology using vegetable oil smoldering, J. Hazard. Mater. 285 (2015) 346–355, http://dx.doi.org/10.1016/j.jhazmat.2014.11.042.

[15] C. Switzer, P. Pironi, J. Gerhard, G. Rein, J.L. Torero, Self-sustaining smoldering combustion: a novel remediation process for non-aqueous-phase liquids in porous media, Environ. Sci. Technol. 43 (2009) 5871–5877, http://dx.doi.org/10.1021/es803483s.

[16] C. Switzer, P. Pironi, J.I. Gerhard, G. Rein, J.L. Torero, Volumetric scale-up of smouldering remediation of contaminated materials, J. Hazard. Mater. 268 (2014) 51–60, http://dx.doi.org/10.1016/j.jhazmat.2013.11.053.

[17] M.A.B. Zanoni, J.L. Torero, J.I. Gerhard, The role of local thermal non-equilibrium in modelling smouldering combustion of organic liquids, Proc. Combust. Inst. (2018) http://dx.doi.org/10.1016/j.proci.2018.05.177.

[18] I. Akkutlu, Y.C. Yortsos, The dynamics of in-situ combustion fronts in porous media, Combust. Flame 134 (2003) 229–247, http://dx.doi.org/10.1016/S0010-2180(03)00095-6.

[19] M. Bazargan, A.R. Kovscek, Pulsating linear in situ combustion: why do we often observe oscillatory behavior?, Comput. Geosci. 22 (2018) 1115–1134, http://dx.doi.org/10.1007/s10596-018-9741-9.

[20] C. Yuan, K. Sadikov, M. Varfolomeev, R. Khaliullin, W. Pu, A. Al-Muntaser, S.S. Mehrabi-Kalajahi, Low-temperature combustion behavior of crude oils in porous media under air flow condition for in-situ combustion (isc) process, Fuel 259 (2020) 116293, http://dx.doi.org/10.1016/j.fuel.2019.116293.

[21] Y. Uchida, K. Kuwana, G. Kushida, Experimental validation of lewis number and convection effects on the smoldering combustion of a thin solid in a narrow space, Combust. Flame 162 (2015) 1957–1963, http://dx.doi.org/10.1016/j.combustflame.2014.12.014.

[22] K. Kuwana, K. Suzuki, Y. Tada, G. Kushida, Effective lewis number of smoldering spread over a thin solid in a narrow channel, Proc. Comb. Inst. 36 (2017) 3203–3210, http://dx.doi.org/10.1016/j.proci.2016.06.159.

[23] O. Zik, E. Moses, Fingering instability in combustion: An extended view, Phys. Rev. E 60 (1999) 518–531, http://dx.doi.org/10.1103/PhysRevE.60.518.

[24] N.V. Agafontsev, D. Kasymov, Estimation of the parameters of combustion of the surface of natural combustible materials by the thermography method, J. Eng. Phys. Thermophys. 93 (2020) 998–1003, http://dx.doi.org/10.1007/s10891-020-02200-w.

[25] D. Drysdale, Spontaneous ignition within solids and smouldering combustion, in: An introduction to fire dynamics, third ed., John Wiley & Sons, Ltd, Chichester, 2011, pp. 317–348, http://dx.doi.org/10.1002/9781119975465.ch8, chapter 8.

[26] B. Hagen, V. Frette, G. Kleppe, B. Arntzen, Transition from smoldering to flaming fire in short cotton samples with asymmetrical boundary conditions, Fire Saf. J. 71 (2015) 69–78, http://dx.doi.org/10.1016/j.firesaf.2014.11.004.

[27] D. Madsen, H.A. Azeem, M. Sandahl, P.van. Hees, B. Husted, Levoglucosan as a tracer for smouldering fire, Fire Technol. 54 (2018) 1871–1885–2782, http://dx.doi.org/10.1007/s10694-018-0773-4.

[28] E. Villacorta, I. Haraldseid, R.F. Mikalsen, B.C. Hagen, S. Erland, G. Kleppe, U. Krause, V. Frette, Onset of smoldering fires in storage silos: Susceptibility to design scenario, and material parameters, Fuel 284 (2021) 118964, http://dx.doi.org/10.1016/j.fuel.2020.118964.

[29] B.C. Hagen, A.K. Meyer, From smoldering to flaming fire: Different modes of transition, Fire Saf. J. (2021) 103292, http://dx.doi.org/10.1016/j.firesaf.2021.103292.

[30] U. Krause, M. Schmidt, The influence of initial conditions on the propagation of smouldering fires in dust accumulations, J. Loss Prev. Process. Ind. 14 (2001) 527–532, http://dx.doi.org/10.1016/S0950-4230(01)00039-0.

[31] K.N. Palmer, Smouldering combustion in dusts and fibrous materials, Combust. Flame 1 (1957) 129–154, http://dx.doi.org/10.1016/0010-2180(57)90041-X.
[32] G. Debenest, V.V. Mourzenko, J.F. Thovert, Smouldering in fixed beds of oil shale grains: governing parameters and global regimes, Combust. Theory Model 9 (2005) 301–321, http://dx.doi.org/10.1080/13647830500098365.
[33] A.G. Merzhanov, B.I. Khaikin, Theory of combustion waves in homogeneous media, Prog. Energy Combust. Sci. 14 (1988) 1–98, http://dx.doi.org/10.1016/0360-1285(88)90006-8.
[34] J.P. Diebold, A.V. Bridgwater, Overview of fast pyrolysis of biomass for the production of liquid fuels, in: Developments in Thermochemical Biomass Conversion, Springer Netherlands, Dordrecht, 1997, pp. 5–23, http://dx.doi.org/10.1007/978-94-009-1559-6_1.
[35] G. Rein, A. Fernandez-Pello, D. Urban, Computational model of forward and opposed smoldering combustion in microgravity, Proc. Combust. Inst. 31 (2007) 2677–2684, http://dx.doi.org/10.1016/j.proci.2006.08.047.
[36] N.C. Roy, Y. Nakamura, Investigation of unsteady behaviors of forward and opposed flow combustion of solid fuel, Combust. Flame 163 (2016) 517–531, http://dx.doi.org/10.1016/j.combustflame.2015.10.030.
[37] M.A. Zanoni, J.L. Torero, J.I. Gerhard, Delineating and explaining the limits of self-sustained smouldering combustion, Combust. Flame 201 (2019) 78–92, http://dx.doi.org/10.1016/j.combustflame.2018.12.004.
[38] P. McCullagh, J.A. Nelder, Binary data, in: Generalized linear models, second ed., in: Monographs on statistics and applied probability, vol. 37, Chapman and Hall, London, 1989, http://dx.doi.org/10.1201/9780203753736, chapter 4.
[39] D. Drysdale, Heat transfer, in: An introduction to fire dynamics, third ed., John Wiley & Sons, Ltd., 2011, pp. 35–82, http://dx.doi.org/10.1002/9781119975465.ch2, chapter 2.
[40] M. Suzuki, R. Dobashi, T. Hirano, Behavior of fires spreading downward over thick paper, Symp. (Int.) Comb. 25 (1994) 1439–1446, http://dx.doi.org/10.1016/S0082-0784(06)80787-3.
[41] K.G. Shkadinskii, B.I. Khaikin, A.G. Merzhanov, Propagation of a pulsating exothermic reaction front in the condensed phase, Combust. Explos. Shock Waves 7 (1971) 15–22, http://dx.doi.org/10.1007/BF00748907.
[42] S. Dosanjh, P. Pagni, A. Fernandez-Pello, Forced cocurrent smoldering combustion, Combust. Flame 68 (1987) 131–142, http://dx.doi.org/10.1016/0010-2180(87)90052-6.
[43] A. Bar-Ilan, G. Rein, A. Fernandez-Pello, J. Torero, D. Urban, Forced forward smoldering experiments in microgravity, Exp. Therm. Fluid Sci. 28 (2004) 743–751, http://dx.doi.org/10.1016/j.expthermflusci.2003.12.012.
[44] A. Bar-Ilan, G. Rein, D. Walther, A. Fernandez-Pello, J. Torero, D. Urban, The effect of buoyancy on opposed smoldering, Combust. Sci. Technol. 176 (2004) 2027–2055, http://dx.doi.org/10.1080/00102200490514822.
[45] J. Buckmaster, D. Lozinski, An elementary discussion of forward smoldering, Combust. Flame 104 (1996) 300–310, http://dx.doi.org/10.1016/0010-2180(95)00124-7.
[46] J. Torero, A. Fernandez-Pello, M. Kitano, Opposed forced flow smoldering of polyurethane foam, Combust. Sci. Technol. 91 (1993) 95–117, http://dx.doi.org/10.1080/00102209308907635.
[47] G. Rein, Smouldering combustion phenomena in science and technology, Int. Rev. Chem. Eng. 1 (2009) 3–18.